

LTCC pion efficiency analysis

A. Bianconi, S. Migliorati

*Università degli Studi di Brescia, Piazza del Mercato 15, 25121 Italy
Istituto Nazionale di Fisica Nucleare, Pavia, Via Agostino Bassi, 6, 27100 Italy*

V. Mascagna

*Università degli Studi dell’Insubria, Como, via Valleggio 11, 22100 Italy
Istituto Nazionale di Fisica Nucleare, Pavia, Via Agostino Bassi, 6, 27100 Italy*

M. Ungaro

Jefferson Lab, 12000 Jefferson Avenue, 23606 Newport News, VA, USA

Abstract

We present here an analysis of the LTCC efficiency in detecting pions. From about 85 million events of the files from skim13 wagon of the spring 2019 RGA data¹, we have selected events with one electron in FD and sectors 1,2,4,6, and a charged particle (“candidate”) in sectors 3 and 5. These events are at a small window at the neutron missing mass to exploit processes where the target proton is converted into a neutron + positive pion. Data show that the LTCC efficiency is an increasing function of the pion energy. The reasons of this behavior have been investigated, and we show that it follows from the larger efficiency of the LTCC at small polar angles.

1 Background

This work continues the analysis of the efficiency of the post-refurbishment LTCC[1]. The efficiency of the detector was first tested with electrons, and then on pions. We have repeated the electron analysis to have a reference, but we will not describe this here and rather concentrate on the pion detection. The electron acceptance is rather constant on a broad range of electron momenta.

In the quoted paper, the LTCC efficiency with pions was not found to be constant as in the electron case, so our work is devoted to a more detailed study of this function. In particular we focus on a systematic study of the dependence of the efficiency on energy and angles, and on explaining the origin of its energy dependence.

2 Methods

From now on, we speak of “reconstruction” meaning all the pieces of the FD (forward detector) of CLAS12, but excluding information coming from LTCC (see [2] for

¹The input file list, the code used for the analysis and all output histograms and tables are available in the [GitHub repository](#)

details on the reconstruction procedure).

A first exploratory analysis on pions was carried on, using events with a charged track identified by the reconstruction as “PID=211”, that is a positive pion. An evident weak point of this analysis is witnessed by fig. 1, where we see the momentum distribution of those pions that have caused the production of *two* photoelectrons in LTCC (this strong requirement reasonably excludes thermal chance photoelectrons).

The presence of a conspicuous component of detected “pions” below the threshold 2.6 GeV/c for the radiation of Cherenkov light by the LTCC suggests that these particles are electrons misidentified as pions.

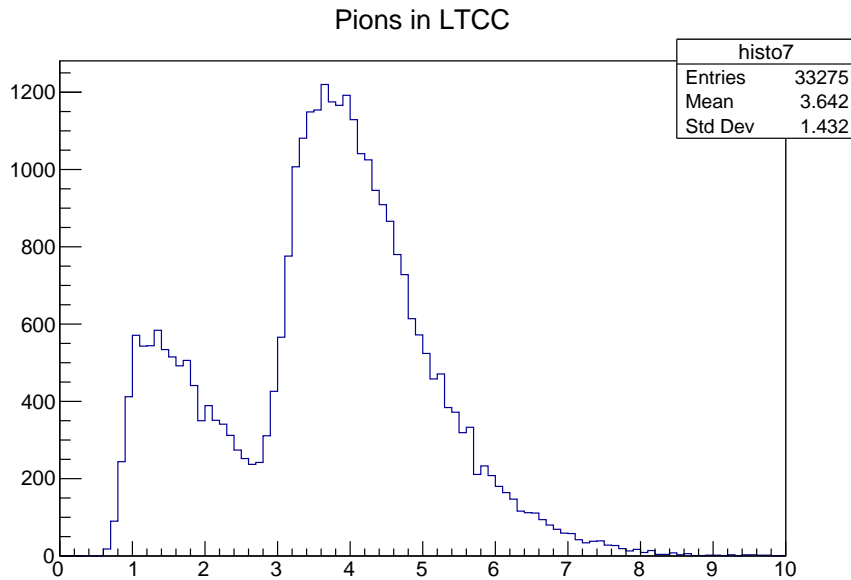


Figure 1: Momentum distribution of particles that the reconstruction has identified as positive pions and have produced two photoelectrons while crossing the LTCC (as described in the text, we use the term reconstruction to indicate all the detectors but the LTCC). An undesired set of “pions” that have produced 2 photoelectrons below the 2.6 GeV/c threshold is well visible. So the analysis we present here contains complications needed to exclude such misidentified particles.

The impossibility of fully trusting the pion/electron separation previously performed by the reconstruction obliges one to look for cuts and kinematic regions where pions are supposed to be the dominant charged particles crossing the LTCC.

This must take into account that the LTCC only covers sectors 3 and 5 of the FD.

The chosen reaction is

$$e + p \rightarrow e + \pi^+ + n \quad (1)$$

that is more specifically reduced to:

$$\begin{aligned} e + p \rightarrow & \text{ semihard electron in } 1, 2, 4, 6 \\ & + \text{ intermediate mass charged in } 3, 5 \end{aligned} \quad (2)$$

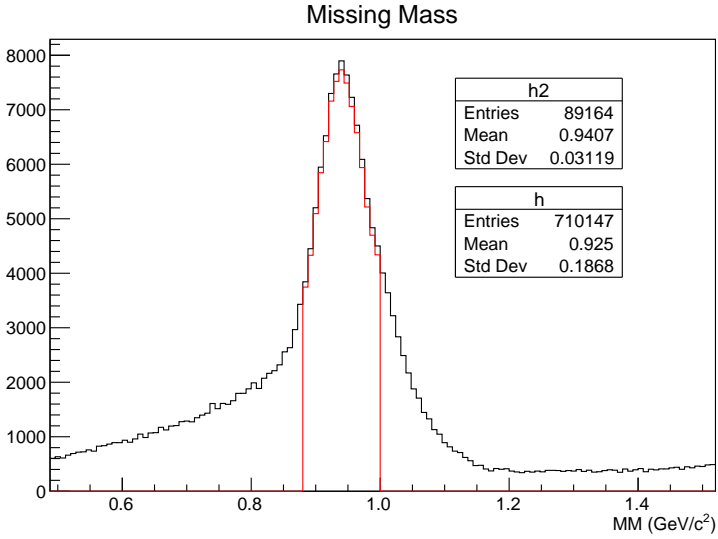


Figure 2: Missing mass distribution for the events of reaction (1), before (black) and after (red) that cuts 2, 3 and 4 described in the text have been applied. The selected events for our analysis are then about 89 000.

where:

- Cut 1. Exactly 2 charged tracks are required in the event. One must be an electron. For its identification we trust the reconstruction PID=11 identification and it must not be in the LTCC sectors 3 and 5.
- Cut 2. The second charged track must be a positive charged particle in sectors 3 or 5.
- Cut 3. The **status** parameter of the detectors must be greater or equal than 2110 to select the topology of the events in a more accurate way; moreover, the absolute value of **chi2pid** must be less than 3 to select more precisely the particles identified by PID (electrons, protons...).
- Cut 4. The missing mass of all the remaining (neutral or undetected) particles must be at the neutron mass peak, within ± 60 MeV ($0.88 \text{ GeV}/c^2 - 1 \text{ GeV}/c^2$).

In Cut 3 we introduced two parameter present in the data: the **status** and the **chi2pid**. Their meaning are the following:

- **status**: defined as the sum of:

$$\begin{aligned}
 & 1000 \times \text{FT} + 2000 \times \text{FD} + 4000 \times \text{CD} + 8000 \times \text{BAND} \\
 & + 100 \times \text{Number of Scintillator responses} \\
 & + 10 \times \text{Number of Calorimeter responses} \\
 & + 1 \times \text{Number of Cherenkov responses}
 \end{aligned}$$

where FT, FD, CD and BAND assume value 1, if the detector subsystem contributed to the particle, or 0 if it does not. It summarizes the topology of the

event using the detectors of CLAS12. Our request (greater than 2110) correspond to have contribution from FD with one calorimeter and one scintillator response.

- `chi2pid`: a signed- χ for the PID identification. It evaluates the quality of the identification of a particle. We take the absolute value and we request it must be less than 3.

We show in figure 2 the missing mass distribution for the events before and after the cuts 2, 3 and 4. The main contribution in the selection of candidates is given by the neutron missing mass cut (Cut 4).

For the left second track in sectors 3, 5, we speak generically of “candidate” although they could possibly be positive particles of several families. The choice of a narrow window at the neutron missing mass should select positive pions.

Our analysis has been carried out on more than 85 million events, that are the events from skim13 group of spring 2019 RGA data. The skim13 wagon (“Missing Neutron Wagon”) selects events with electrons momentum $p_e = 0.5 \text{ GeV}/c - 7.5 \text{ GeV}/c$, high-momentum positive-charged particles ($p_{q+} > 3.5 \text{ GeV}/c$) and with the condition that the missing mass of an electron and of another particle in the event list is on the neutron peak when all the other final particles are neglected. For details, see the [Missing Neutron Wagon code](#). Our cuts have reduced these events to a much smaller number ($\sim 89\,000$), visible in the statistical panel of each figure.

3 Results

Our standard presentation for 1D-distributions consists of 4 histograms:

- The number of candidates in the LTCC for sectors 3 and 5, separately. Three distributions are showed: the total number of candidates (black) and the number of candidates with at least one (blue) or two (red) photoelectrons associated.
- The ratio of the signal-associated candidates and total candidates in LTCC. This is what we term “efficiency”. This is done separately for sector 3 and 5 and for one (blue) and two (red) photoelectrons signals.

First, we show these distributions as functions of the candidate momentum P , in fig. 3.

Two observations on this figure. First, there are no more “pions” detected below the pion threshold $2.6 \text{ GeV}/c$. This means that the adopted cuts are effective at keeping electrons and positrons away. Second, the efficiency increases with the candidate energy. This is related to the LTCC geometry.

Another observation is related to the statistics of the two sectors. A difference of more than 10 % between the number of candidates in sector 3 and 5 is present. In particular, sector 5 seems to see more candidate particles than sector 3 (see the statistics panels in fig. 3 and successive).

Next, we show the candidate populations and efficiency distributions as functions of the vertex angles θ (polar, fig. 4) and ϕ (azimuthal, fig. 5). Concerning the θ -distributions, apart from evident differences between the efficiency in sectors 3 and 5,

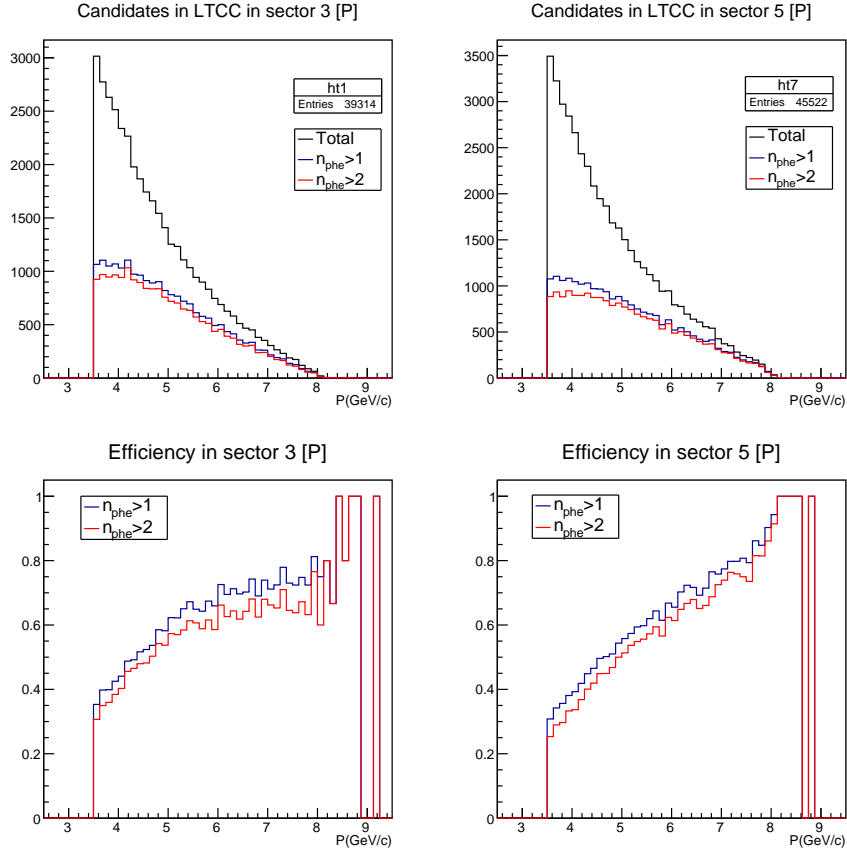


Figure 3: Top Left: Number of candidates that cross the LTCC sector 3; three histograms are represented: total number of candidates (with or without a signal in the LTCC), and number of candidates with a signal 1 or 2 photoelectrons. Top Right: The same distributions as before for sector 5. Bottom: Ratio of the previous two distributions (efficiency) for sector 3 and 5. In each bin this is the ratio of the candidates that have produced photoelectrons to all those crossing the LTCC. The evident increase of the efficiency at large energies is discussed in the last section of this report.

a series of systematic irregularities is visible in both. Both sectors present gap/peak alternations that cannot be explained as statistical fluctuations. They origin in the periodic pattern of the photomultiplier+mirrors detector geometry. Concerning the ϕ -distributions, a better efficiency is evident in proximity of the detector edges. This is due to the nearness of the tracks and the positions of PMs, as discussed in Section 4.

To simultaneously show the θ, ϕ distributions, we have reported in fig. 6 candidates populations (candidates in sectors 3 and 5, candidates with more than 2 photoelectrons associated) and efficiency (for both sectors) distributions in terms of both vertex angles in two dimensional histograms.

Some well visible difference is present between the total outcomes of regions 3 and 5, but this mainly concerns the number of candidates that cross regions 3 and 5.

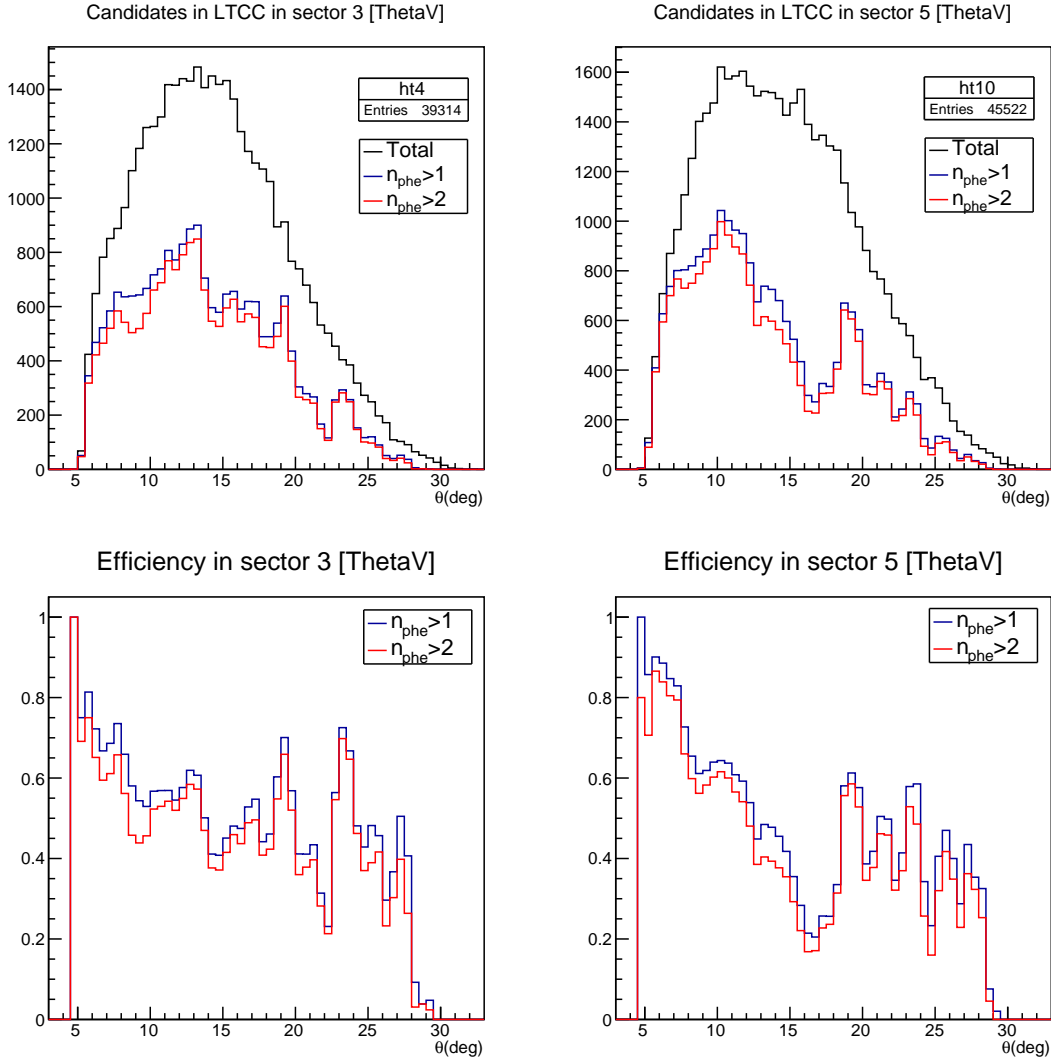


Figure 4: The same distributions as in fig. 3, but as functions of the vertex polar angle of the candidate.

We also considered the evaluation of efficiency as a function of transverse coordinates at the detector (local coordinates). Two pairs of local coordinates are available:

1. Hit coordinates, associated with the place where the particle has hit the LTCC that are in bank `REC::Cherenkov`, methods `che(LTCC)->getX()` / `getY()`. In most cases these are identified with the positions of the PM's, at the edges of each sector of the LTCC.
2. Cross coordinates, associated with the place where the track reconstruction interpolates the candidate passage through the LTCC. These are from the bank the bank `REC::Traj`, methods `traj(LTCC,1)->getX()` / `getY()`.

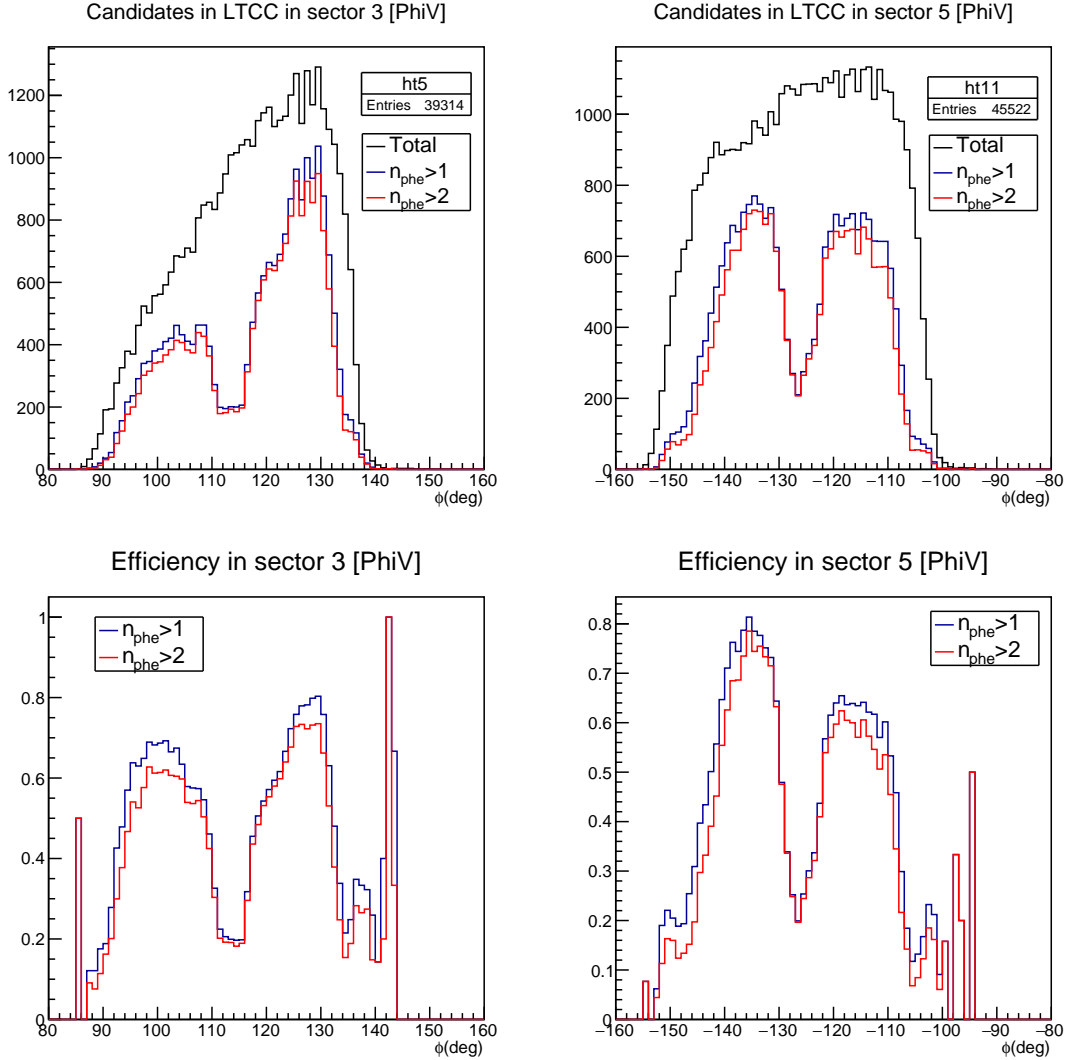


Figure 5: The same distributions as in fig. 3, but as functions of the vertex azimuthal angle of the candidate.

In fig. 7 we checked the efficiency in terms of LTCC local cross coordinates. We called these coordinates X (`traj(LTCC,1)->getX()`) and Y (`traj(LTCC,1)->getY()`).

This figure is useful to understand the origin of irregularities in angles distributions.

We have also checked the 2-dimensional distribution of the transverse hit coordinates x, y of a particle when crossing the LTCC (red markers in fig. 8) compared to the cross coordinates (black markers, same figure).

These show that a particle does not really need to hit a PM, but is more likely to be detected by the LTCC if its track is closer to the PM's.

Moreover, the areas of the LTCC detector where the red markers are absent or

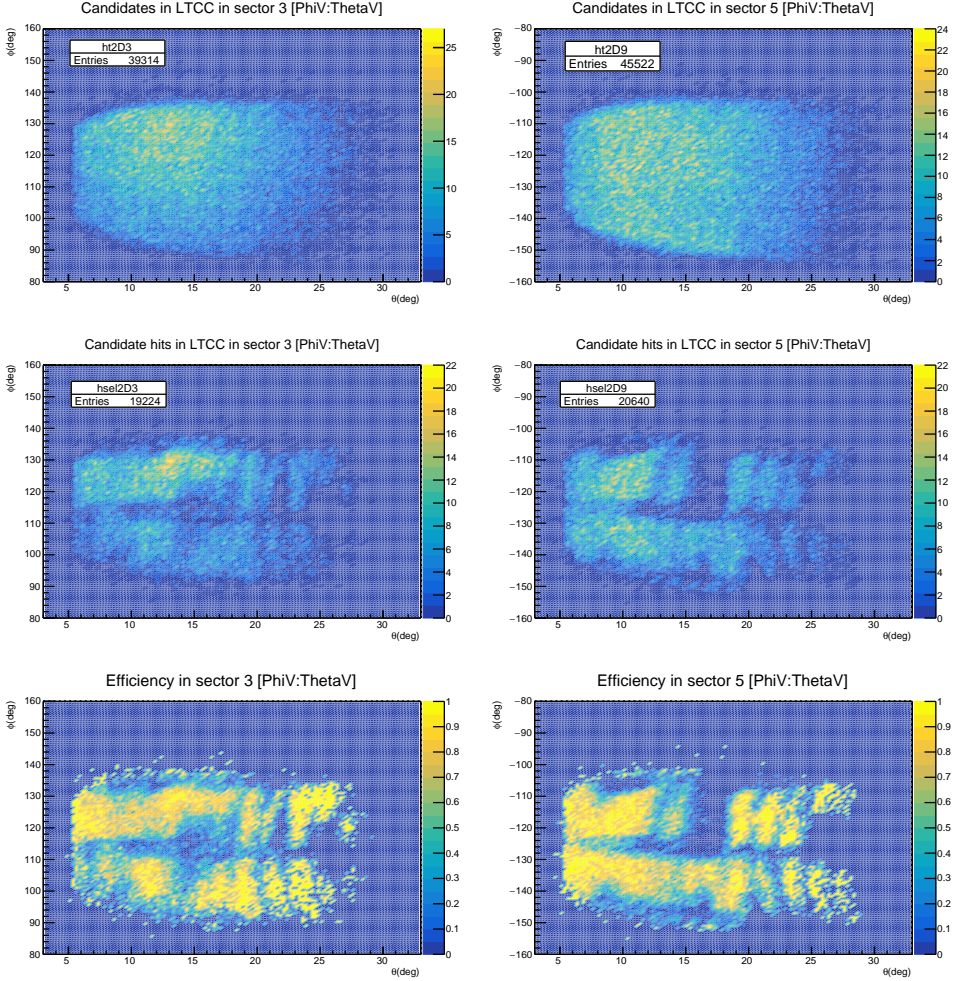


Figure 6: First row panels: Total vertex polar and azimuthal angles distributions of the candidates for sectors 3 and 5; Second row panels: Candidates with a signal of more than 2 photoelectrons in LTCC, sectors 3 and 5; Third row panels: Efficiency for sectors 3 and 5.

low in number almost coincides with the regions where the cross coordinates (black markers) are absent too.

The detailed results of the present analysis are presented in two long tables, available in the [GitHub repository](#) of the present work. These tables contain the efficiency values for sectors 3 and 5 in P , θ and ϕ . The central values for the bins of these variables are used. To calculate them we used the same method to plot the previous histograms: we realized the distributions in 3D-space (P , θ , ϕ) using a 3D-histogram for candidates that crossed LTCC, for candidates with a signal ($n_{phe} > 2$) in LTCC and finally divided these two histograms, obtaining the efficiencies for sectors 3 and 5.

We also checked the average number of photoelectrons revealed for sector 3 and

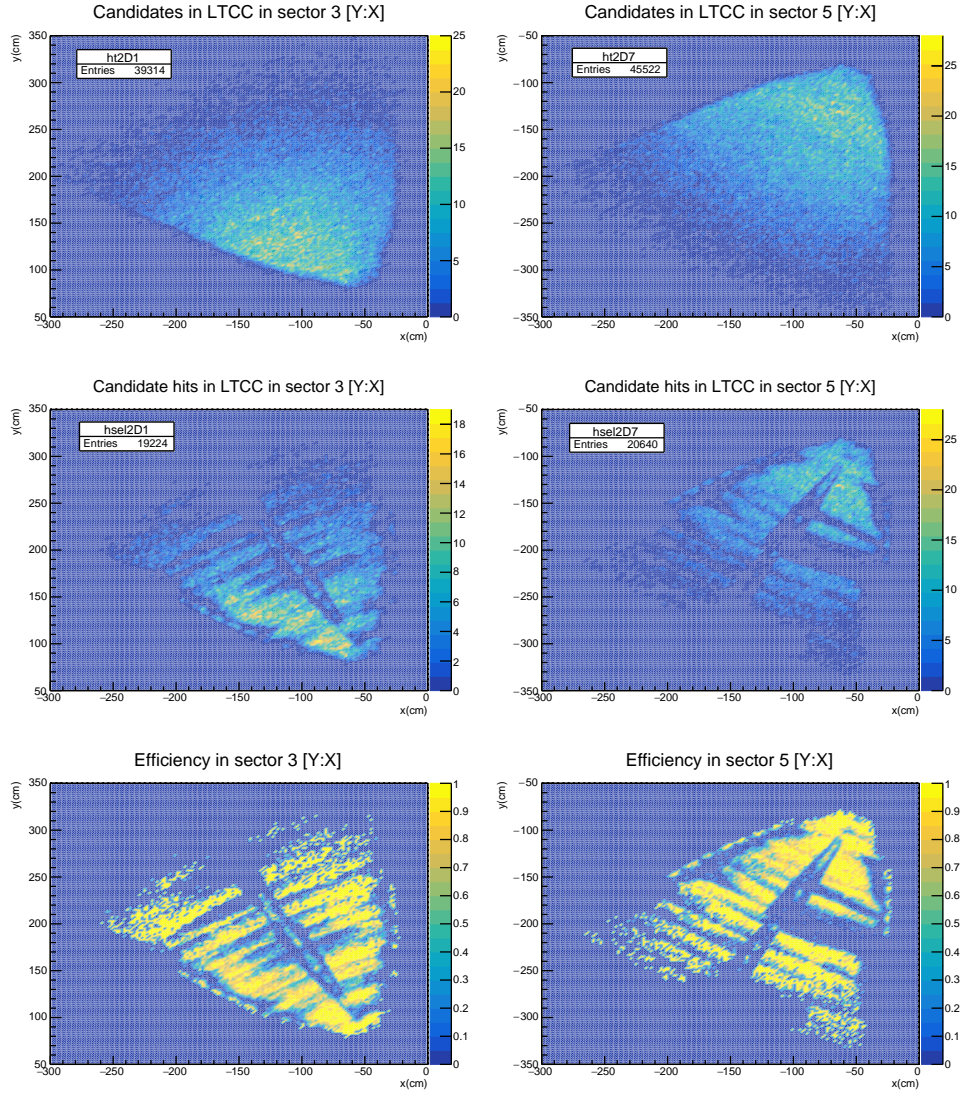


Figure 7: The efficiency map for LTCC detector coordinates X and Y. One can notice the sectors substructures from the last two panels.

5, in dependence of the angles, in Fig. 9. Apart from an anomalous number of photoelectrons, due to a noisy PMT in sector 3 (right-side), the rest of the detector seems to work correctly.

4 Discussion

Geometry and increase of the LTCC response at increasing candidate energies

The figures 4 and 6 on angular efficiency ratio, joined with the fact that the most energetic pions concentrate at small polar angles, suggest that geometry is essential

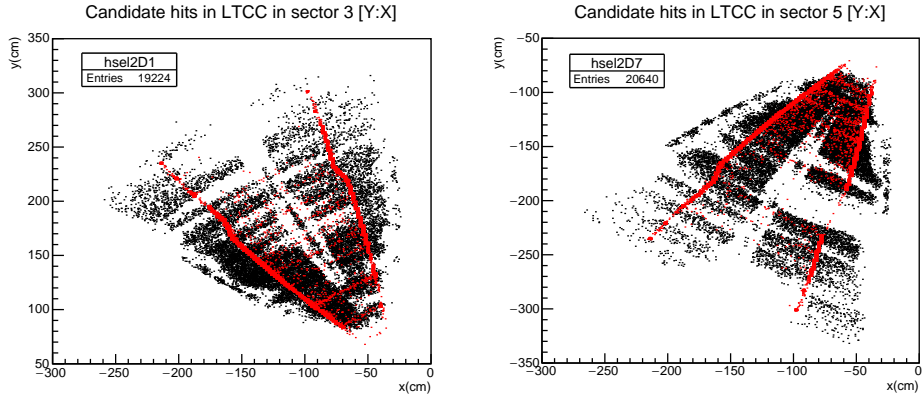


Figure 8: Cross coordinates (black markers) and hit coordinates (red markers) for sectors 3 (left) and 5 (right), with associated a 2-photoelectrons signal in LTCC. Both these pairs of coordinates are local (at LTCC), only indirectly related to the vertex angles. The PM positions and the hit coordinates are correlated for definition. A correlation between absence of both hit and cross coordinates in some region of the detector can be noted, especially in the right panel.

in contributing to the energy efficiency.

In particular, the θ distribution shows that the LTCC efficiency is markedly biased towards small polar angles.

Now the point is that while the cross section of the PM's is independent of θ (each pair of PM's corresponds to the same $\Delta\theta$), the area in between two opposite side PM's is $\propto \theta$. So the chances for a candidate to be close to a PM decrease at increasing θ . On the other side, the energy distribution of the pions is not angle-independent. This correlation is better shown in our last figure, fig. 10. The candidates above the LTCC threshold form an oblique belt where we have a strong correlation between angle and energy: the smaller the angle, the larger the energy. This explains the increase of the LTCC efficiency shown in our previous figure 3.

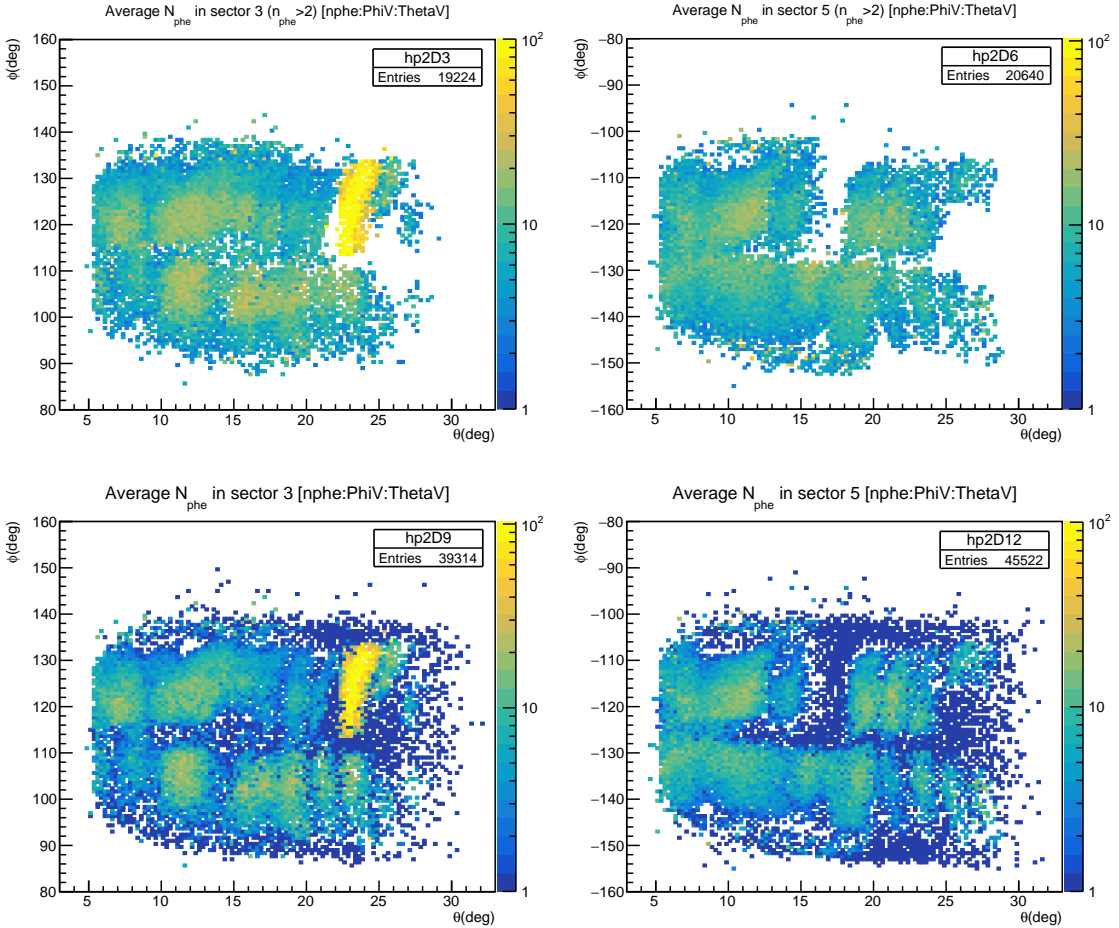


Figure 9: Average number of photoelectrons in dependence of (θ, ϕ) . The first row of figures is for $n_{phe} > 2$, while the second one is for $n_{phe} \neq 0$. The anomalous high number of photoelectrons in sector 3 is due to a noisy PMT. However, this behavior does not seem to affect the efficiency of this element of the detector, since what is really relevant is the frequency of events where at least one photoelectron is produced, and this is not larger than in other good-efficiency elements of the LTCC.

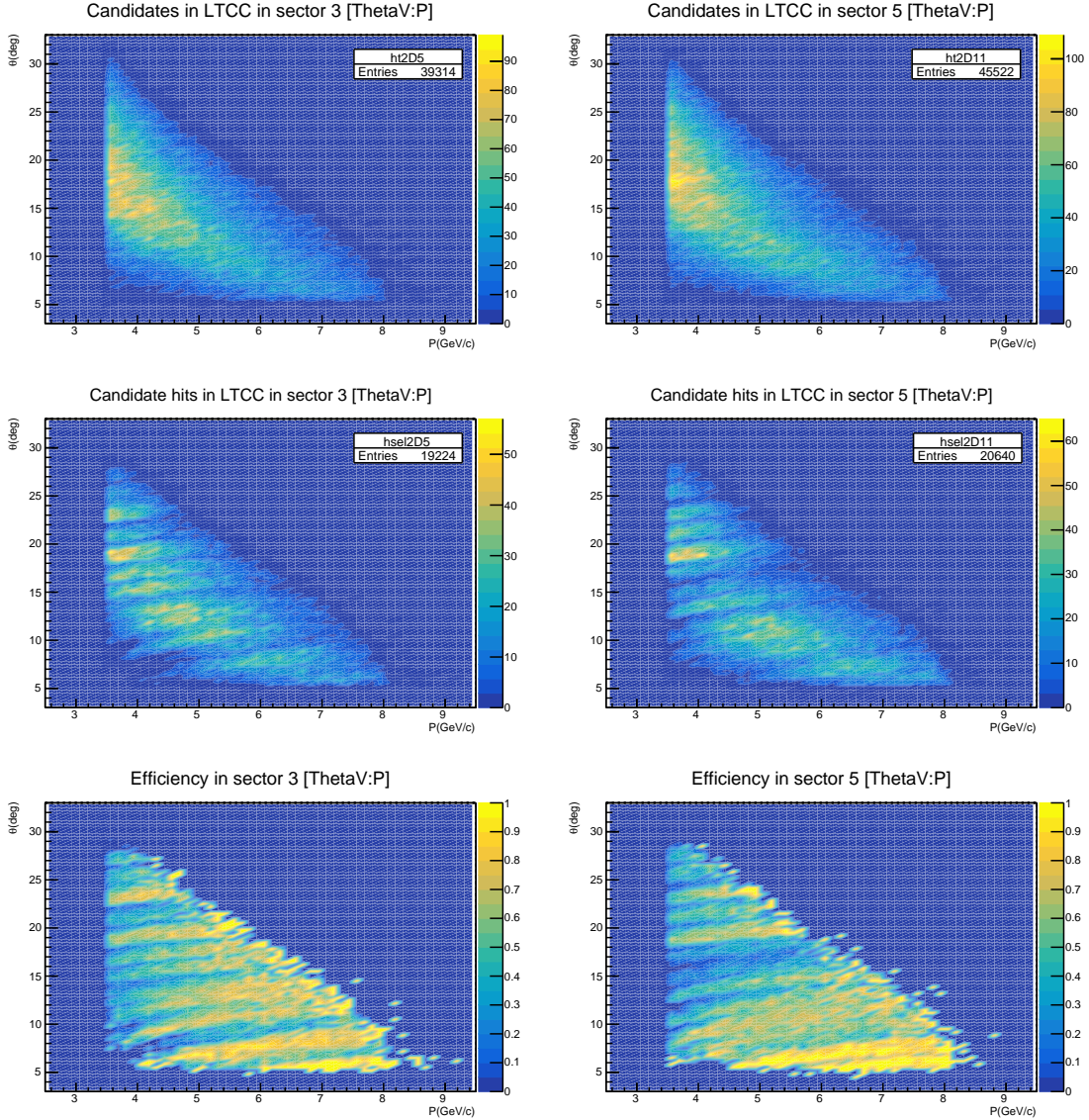


Figure 10: The usual 6 histograms (candidates, candidates with 2 photoelectrons, efficiencies in sectors 3 and 5) in terms of the candidate P and θ . A energy-angle correlation is visible since the very first panel: the larger P , the smaller the angle. This correlation is present in the following panels too, although partly masked by periodic angular patterns related to the PM regular arrangement. This correlation causes the candidates with larger energies to be in polar angle regions where the LTCC is more efficient, although with local irregularities.

References

- [1] M. Ungaro et al. “The CLAS12 Low Threshold Cherenkov detector”. In: *Nuclear Instruments and Methods in Physics Research Section A: Accelerators, Spectrometers, Detectors and Associated Equipment* 957 (2020), p. 163420. ISSN: 0168-9002. DOI: <https://doi.org/10.1016/j.nima.2020.163420>. URL: <https://www.sciencedirect.com/science/article/pii/S0168900220300255>.
- [2] V. Ziegler et al. “The CLAS12 software framework and event reconstruction”. In: *Nuclear Instruments and Methods in Physics Research Section A: Accelerators, Spectrometers, Detectors and Associated Equipment* 959 (2020), p. 163472. ISSN: 0168-9002. DOI: <https://doi.org/10.1016/j.nima.2020.163472>. URL: <https://www.sciencedirect.com/science/article/pii/S0168900220300784>.